Journal of Vacuum Science and Technology A

RESEARCH ARTICLE | FEBRUARY 12 2024

Characterization of elastomer degradation in O_2/Ar plasma via mass and surface morphology changes

Nicholas Connolly ; Michael Hysick ; David E. Barlaz ; Raquel Garza ; Gilberto Lunardi ;
David N. Ruzic

J. Vac. Sci. Technol. A 42, 023004 (2024)
https://doi.org/10.1116/6.0003240

CrossMark

12 February 2024 19:37:45

JVST A
Journal of Vacuum Science & Technology A
ARTICLE
pubs.aip.org/avs/jva

Characterization of elastomer degradation in O_2/Ar plasma via mass and surface morphology changes

Cite as: J. Vac. Sci. Technol. A **42**, 023004 (2024); doi: 10.1116/6.0003240
Submitted: 25 October 2023 · Accepted: 12 January 2024 ·
Published Online: 12 February 2024

View Online

Export Citation

CrossMark

Nicholas Connolly,[1] Michael Hysick,[1] David E. Barlaz,[2] Raquel Garza,[1] Gilberto Lunardi,[3] and David N. Ruzic[1,a)]

AFFILIATIONS

[1]Center for Plasma-Material Interactions, Department of Nuclear, Plasma, Radiological, and Engineering, University of Illinois at Urbana-Champaign, Urbana, Illinois 61801
[2]TEL Technology Center, America, LLC, Albany, New York 12203
[3]DuPont Electronics and Industrial, Newark, Delaware 19713

Note: This paper is part of the Special Topic Collection Celebrating the Achievements and Life of Joe Greene.
[a)]**Author to whom correspondence should be addressed:** druzic@illinois.edu

ABSTRACT

The degradation of fluoroelastomer, perfluoroelastomer (FFKM), and fluorosilicone materials were compared between three O_2/Ar plasma conditions: full plasma (ions plus radicals), radical only, and ion only. These elastomer materials are used extensively in plasma processing equipment used to manufacture semiconductors, and understanding the plasma environments that enhance degradation will inform material choice and further material development. Langmuir probe measurements were made to quantify the electron temperature and plasma density; radical probe measurements were made to quantify the oxygen radical density. The results suggested that plasma radicals were required to drive significant mass loss rates, with ions speeding up the mass loss rate further in the full plasma case. Additionally, it was determined that plasma radicals were the main driver of surface changes of the elastomer, with similar surface roughening in plasma versus radical only conditions and less significant roughening in ion-only conditions. The O_2/Ar plasma discharge had an electron temperature of 4.6 ± 0.1 eV and a plasma density of $2.9 \pm 0.07 \times 10^{16}\,\mathrm{m}^{-3}$. It was observed that the fluorosilicone material had the lowest mass loss rate, the unfilled FFKM had the highest mass loss rate, and the silica-filled FFKM had the lowest mass loss rate among the FFKMs tested. The presence of oxygen radicals during exposure conditions significantly changed surface roughness.

Published under an exclusive license by the AVS. https://doi.org/10.1116/6.0003240

12 February 2024 19:37:45

I. INTRODUCTION

Plasma processing equipment used to manufacture semiconductors utilizes relatively corrosive chemistries, including halogens, oxygen, or a mixture of both.[1,2] Elastomer seals (aka O-rings) are necessary and important parts of plasma processing equipment and are chosen over metal seals due to the ability to break and remake the seals without replacement, undesirable byproducts of metal seals (such as copper) for defectivity considerations, and general volatility of elastomer seal byproducts. Due to the corrosive plasma environment, a high level of chemical resistance is required of the elastomer seals.[3] Depending on the location of the seal in the processing chamber, it may be exposed to plasma, which includes both ions and radical species, or a predominantly radical-rich environment. Without adequate plasma resistance, the seals will degrade over time, with risks being the failure of the seal or chamber contamination from seal degradation byproducts.[4] Any seal will have a finite lifetime in plasma processing equipment, but utilizing seals with lifetimes that do not dictate chamber maintenance frequencies is an obvious goal.

Perfluoroelastomer (FFKM), fluoroelastomer (FKM), and fluorosilicone (FVMQ) materials are top choices for elastomer materials in plasma processing equipment due to their resistance to chemical attack, heat, or both of these factors.[5,6] Table I lists common fluorocarbon monomers used to create fluorinated elastomers, and Fig. 1 details typical structures of the base polymer for each material type, known as the backbone.[7] The backbone makes up a large majority of the elastomer material, with the cure-site monomer, fillers, and any other additives making up the balance of the ingredients for producing the elastomer.

Published under an exclusive license by the AVS

TABLE I. Common fluorocarbon monomers used to create fluorinated elastomers.

Structure	Name	Symbol
$CH_2{=}CF_2$	Vinylidene fluoride	VF2
$CF_3CF{=}CF_2$	Hexafluorpropylene	HFP
$CF_2{=}CF_2$	Tetrafluoroethylene	TFE
$CF_3OCF{=}CF_2$	Perfluoromethylvinyl Ether	PMVE
$CF_3(CF_2)_zOCF{=}CF_2$	Perfluoroalkylvinyl Ether	PAVE
$ClCF{=}CF_2$	Chlorotrifluoroethylene	CTFE
$CH_2{=}CH_2$	Ethylene	E
$CH_3CH_2{=}CH_2$	Propylene	P

FFKMs are widely used in semiconductor wafer processing equipment because of their superior resistance to chemical attack and heat, with maximum service temperatures as high as 316 °C.[8] The broad resistance of FFKMs to degradation is due to the completely fluorinated backbone, as shown in Fig. 1(a); the backbone has no C—H bonds, only C—F bonds. Full fluorination provides the highest resistance due to multiple factors: the carbon—fluorine bond is the most stable single bond and the steric "shielding effect" by fluorine atoms both protects the C—C bond in the polymer backbone and evens charge distribution.[8,9] The second class of materials widely utilized in plasma environments are fluoroelastomers (FKMs). Unlike FFKMs which only have one specific backbone structure, there can be multiple backbone structures of FKMs, as shown in Fig. 1(b). The common feature of FKMs is that they contain some level of C—H bonds along with C—F bonds—in other words, partial fluorination. Because they are only partially fluorinated, they have some resistance to chemical attack and heat, but not to the same degree as FFKMs. The third class of materials utilized in plasma environments is fluorosilicones (FVMQs), as shown in Fig. 1(c). Silicone elastomers in general have a linear alternating sequence of silicon and oxygen atoms instead of a carbon chain in their backbone, with FVMQs specifically having partially fluorinated comonomers that increase chemical resistance. FVMQs are considered for oxygen plasma processes due to their resistance to degradation in that environment.[10]

In general, there are few peer-reviewed studies that investigate the degradation of semiconductor industry relevant elastomers, despite the importance of their resistance to the relatively harsh semiconductor environments. One recent study investigated the plasma resistance of an FFKM and FKM material in a CF_4/O_2 plasma environment and noted a similar lack of fundamental studies of semiconductor industry relevant plasma interactions with elastomers.[4] Elastomer suppliers periodically publish plasma resistance data; these studies generally compare mass loss of various materials at a chosen recipe, but do not include plasma diagnostics.[1,8,11,12] To start to fill this gap, this study investigates the fundamental differences in elastomer degradation between three plasma system cases: full plasma (ions plus radicals), radical only, and ion only. The industrially relevant O_2/Ar plasma chemistry is chosen, and plasma diagnostics are used to determine the plasma electron temperature (T_e), plasma density (n_e), and oxygen radical density (n_O). The elastomers are characterized by mass loss rate and surface roughness change after exposure.

II. EXPERIMENT

A. Equipment

The experiment was completed on the Plasma-Materials Interaction Chamber (PMIC) at the University of Illinois Urbana-Champaign (Fig. 2). The PMIC contains a MØRI-200 helicon plasma source, elastomer sample stage, pumping system, and a gas delivery system. A schematic of the PMIC is shown in Fig. 3.

The PMIC utilized a MØRI-200 helicon plasma source at 13.56 MHz frequency, with an RF generator capable of power delivery from 0 to 3 kW, and a matching network contained inside the

12 February 2024 19:37:45

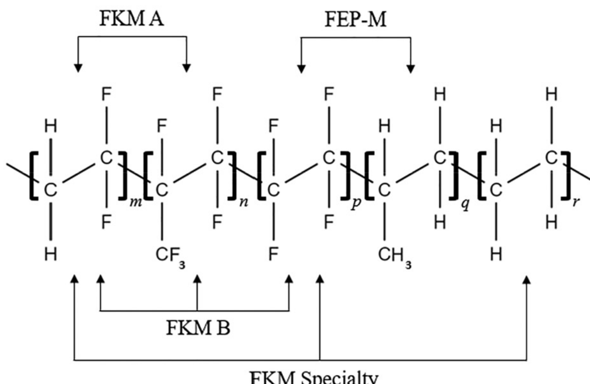

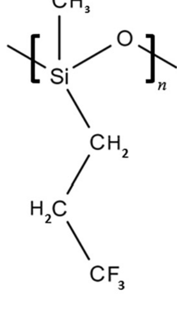

FIG. 1. Typical backbone structure of (a) perfluoroelastomers, for which PMVE is the most commonly used ether monomer; (b) fluoroelastomers, with some common backbones specified; and (c) fluorosilicones.

Published under an exclusive license by the AVS

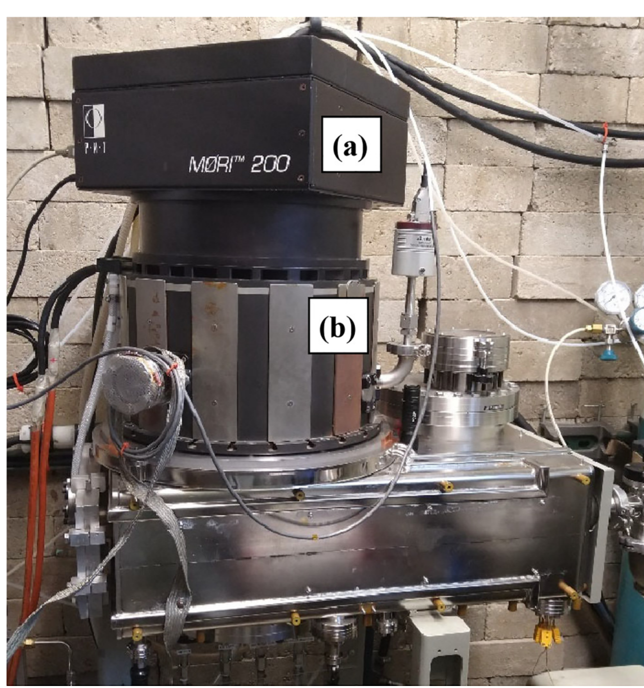

FIG. 2. PMIC at the University of Illinois Urbana-Champaign. The (a) antenna/electromagnet assembly contains the plasma source and the (b) multipole magnetic bucket is the process chamber containing substrates for exposure.

antenna assembly to minimize reflected power. The bell jar is surrounded by a double loop antenna, with diameter of 110 mm and axial spacing of 150 mm. The antenna was designed such that the loops have a 180° phase difference. The bell jar and antenna are surrounded by coplanar electromagnets that produce a diverging magnetic field; the magnetic field is largest in the bell jar region and decreases rapidly in the axial direction into the chamber. The process chamber utilizes multipole magnets on its outer diameter to limit radial diffusion of plasma to the chamber walls.[13] The gas flow into the chamber was controlled by mass flow controllers (MFCs). A corrosion-resistant, dry rough vacuum pump was used to reach adequate processing pressures, with a throttle valve to control chamber pressure. A capacitance manometer was used to measure pressure in the chamber. The chamber is capable of operating at pressures typical of inductively coupled plasma (ICP) chambers, in the range of approximately 5 mTorr to a few hundred mTorr. The chamber base pressure was 1 mTorr at the operating throttle positions. Therefore, even without a turbomolecular pump, the contamination fraction during experimental runs was $\leq$1%.

A sample plate was constructed from aluminum, with grooves cut to fit pieces of AS568-214 O-rings; the sample plate was designed so that the O-rings are not under any compression in any direction. Figure 4 shows the sample plate with O-rings loaded in before an exposure. The sample plate sits on a stage that has the capability for heating up to the max operating temperature of the O-rings. The O-rings are placed 13 cm below the bell jar to mimic the generally radical-rich environments of O-rings in commercial semiconductor fabrication equipment.

12 February 2024 19:37:45

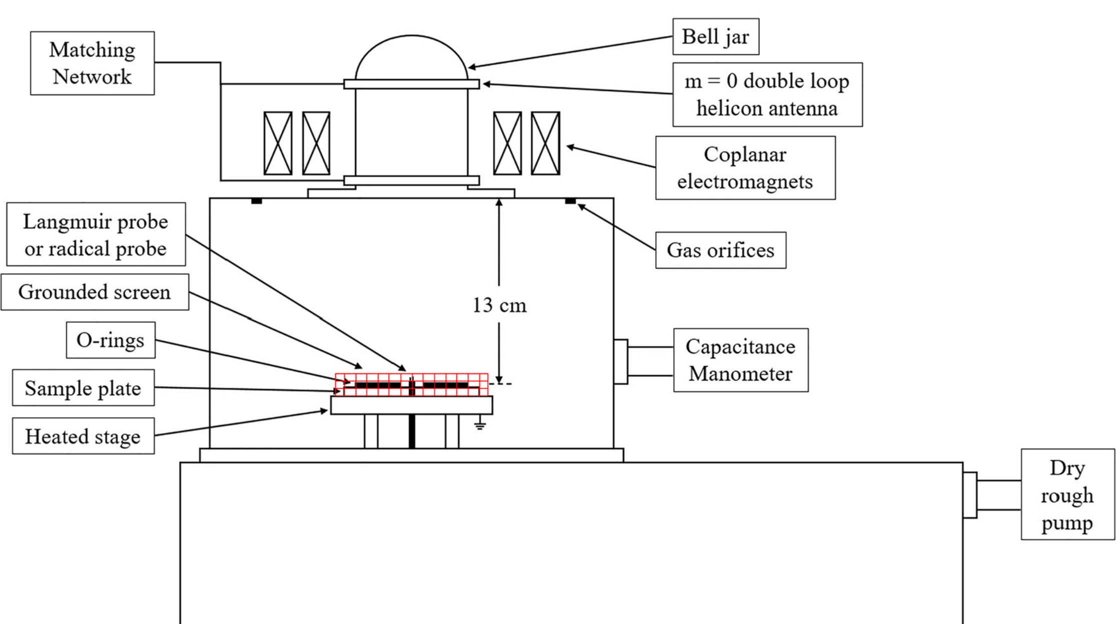

FIG. 3. Schematic of the PMIC. The plasma is created inside the bell jar and diffuses into the process chamber. The O-rings were placed 13 cm below the bell jar. A grounded screen was placed over the O-ring sample plate when running radical only exposures. When taking Langmuir probe or radical probe measurements, the probes were set to the same height as the O-ring samples, using an annular grounded plate to mimic the heated stage and sample plate.

Published under an exclusive license by the AVS

FIG. 4. Sample plate with O-rings loaded before exposure.

B. Procedure

Six elastomer materials were chosen for this study: four FFKM materials, one FKM material, and one fluorosilicone material. Table II lists the material name used to identify the material, its material class, primary filler, color, maximum service temperature as recommended by the manufacturer, and hardness (shore A). These O-ring materials were chosen for testing because they spanned a wide range of classes, primary fillers, and other characteristics for which it was expected that the plasma exposure will have different effects. In general, due to their level of fluorination, FFKM materials have the highest plasma resistance in fluorinated gas plasmas, but other O-ring types may perform better in specific plasma chemistries.

The goal of this study was to compare O-ring degradation in three types of O_2/Ar plasma environments: radical only, full plasma (ions plus radicals), and ion only. The experiment setpoints tested to achieve this comparison are shown in Table III. The RF power delivered to the plasma was held constant at 750 W for all runs, the chamber pressure was held constant at 100 mTorr, and the exposure time was 5 h for all tests. The total flow was held constant at 33 standard cubic centimeters per minute (SCCM), with 27 SCCM of O_2 and 6 SCCM of Ar when running an O_2/Ar chemistry. The temperature of the stage was not controlled, and, therefore, any increase above room temperature was due to heating from the plasma. The maximum temperature reached during the tests had a relatively small range of 22 °C and was at least 90 °C lower than the max service temperature of the materials, so it was assumed that controlling the stage temperature was not necessary. To ensure that only radicals were reaching the O-rings in the radical only exposure, a grounded mesh was placed on top of the sample plate to screen out ions.

TABLE III. Experimental setpoints for plasma exposures.

Setpoint	Radical only (O)	Plasma (O_2/Ar)	Ion only (Ar)
Power (W)	750	750	750
Pressure (mTorr)	100	100	100
Total flow (SCCM)	33	33	33
O_2 flow (SCCM)	27	27	0
Ar flow (SCCM)	6	6	33
Exposure time (h)	5	5	5
Max. temperature Reached (°C)	85	83	63
Grounded screen over samples	Yes	No	No

The O_2/Ar electron temperature (T_e), plasma density (n_e), and oxygen radical density (n_O) were characterized at the sample location, with a grounded plate in the same location as the sample plate and heated stage to mimic the exposure environment. T_e and n_e were characterized using an RF-compensated single Langmuir probe (Impedans Ltd. probe part No. 02-0144-02 and Impedans Ltd. electronics unit part No. 02-0045-04). n_O was determined using a catalytic radical probe system. Figure 3 shows the location of the probes in the chamber, both taking measurements in the plasma 13 cm below the bell jar.

The method for determining n_O using a catalytic radical probe system is described in Qerimi *et al.*[14,15] In this method, the radical probe consists of two stainless-steel thermocouples placed next to each other in the plasma. One thermocouple has a catalytic material coated on the probe tip, while the other is left as bare stainless steel. When the thermocouple tips are kept in close proximity in the plasma environment, all heating and cooling mechanisms are the same except for the heat generated due to recombination of

12 February 2024 19:37:45

TABLE II. Exposed O-ring material information.

Material name	FFKM_SiO_2	FFKM_CB	FFKM_TiO_2	FFKM_UF	FKM_CB	FS_PM
Class	FFKM	FFKM	FFKM	FFKM	FKM	FVMQ
Primary filler	SiO_2	Carbon black	TiO_2	Unfilled	Carbon black	Pigment
Color	White	Black	White	Black	Black	Blue
Maximum service temperature (°C)	260	275	315	275	200	175
Hardness (Shore A)	80	75	75	55	75	70

Published under an exclusive license by the AVS

radicals, because that will be dependent on the material. Therefore, a temperature difference will develop between the two probes, and that temperature difference is proportional to the radical density in the plasma. Equation (1) shows the relationship between temperature difference and radical density, where n is the radical density, S is the cross-sectional area of the probe, χ is the thermal conductivity of stainless steel, W_D is the dissociation energy of the parent molecule, v is the thermal velocity of radicals, A is the surface area of the catalytic material, L is the length of the probe, T is the temperature, and γ is the recombination coefficient of radicals on the catalytic surface,

$$n = \frac{8S\chi}{W_D vAL}\frac{T_{\text{Probe A}} - T_{\text{Probe B}}}{\gamma_{\text{Probe A}} - \gamma_{\text{Probe B}}}. \quad (1)$$

Copper was used as the catalytic coating for oxygen radical measurement because oxygen has a high recombination coefficient on copper relative to stainless steel. The thermocouples used were 0.51 mm in diameter, yielding a cross-sectional area, S, of $2.0 \times 10^{-7}\,\text{m}^2$. The thermal conductivity of stainless steel, χ, is 15 W/m/K.[16] The dissociation of the O_2 molecule, W_D, is 5.2 eV.[17] The O radicals are assumed to be in thermal equilibrium with the neutral gas at 0.025 eV (room temperature), yielding a thermal velocity of 617 m/s. The coating length of copper was 2 mm, yielding a catalytic material surface area, A, of $3.4 \times 10^{-6}\,\text{m}^2$. The length of the probe, L, was 0.15 m. The recombination coefficient of O radicals on copper, γ_{Cu}, is 0.31 and the recombination coefficient of O radicals on stainless steel, γ_{SS}, is 0.07.[14]

The O-ring degradation was characterized using two methods: mass loss and surface roughness. An analytical balance was used to measure each sample before and after exposure to determine the mass loss during exposure. An optical profilometer (Keyence VK-X1000 3D Laser Scanning Confocal Microscope) was used to characterize the surface roughness of the O-rings before and after exposure; the surface roughness parameter reported was the root mean square height, S_q.

III. RESULTS AND DISCUSSION

A. Plasma characterization results

The RF-compensated, single Langmuir probe was used to collect a current versus voltage trace in the plasma condition from Table III at the O-ring sample location (see Fig. 3). The electron temperature (T_e) was determined by analyzing the slope of a linear approximation of the natural log of the electron current versus the difference of plasma potential and probe voltage; T_e equals the negative reciprocal of the slope. The Laframboise method was used to determine plasma density (n_e), as sheath size and sheath collisionality affect the analysis of the collected current.[18] T_e was determined to be 4.6 ± 0.1 eV and n_e was determined to be $2.9 \times 10^{16} \pm 0.07 \times 10^{16}\,\text{m}^{-3}$. Although this plasma source is capable of higher plasma densities, because of the relatively high pressure and measurement location far from the bell jar, the determined density is not unexpectedly low. A representative current versus voltage trace and natural log of the electron current versus the difference of plasma potential and probe voltage are shown in the Appendix.

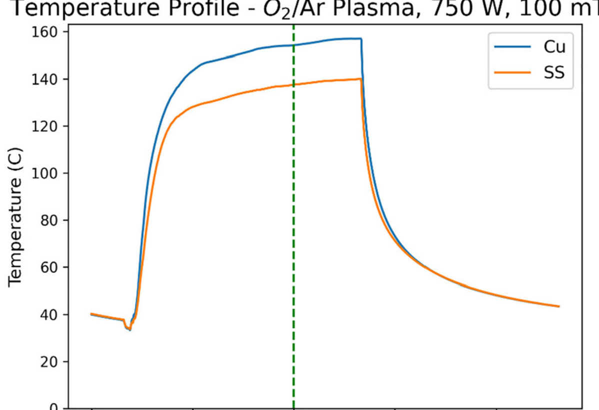

FIG. 5. Temperature vs time of representative radical probe run in plasma condition from Table III: power = 750 W, pressure = 100 mT, O_2 flow = 27 SCCM, and Ar flow = 6 SCCM. For reference, the temperature difference at the green dotted line is 16.6 °C.

The catalytic radical probe system was used to measure the oxygen radical density (n_O) at the O-ring sample location, identical to the Langmuir probe location shown in Fig. 3. As with the Langmuir probe, the radical probe measured the plasma condition from Table III.

The plasma was run until the temperature difference of the probes reached a steady state; Fig. 5 shows the temperature profile from a representative radical probe run. The probe was also run in an argon-only plasma, to determine if there was a steady state temperature difference in a chemically inert environment, indicative of small differences in heating or cooling between the two probes. The temperature difference during the argon-only run was then subtracted from the temperature difference during the plasma condition run. The mean temperature difference between the Cu-coated thermocouple and the bare stainless-steel thermocouple across three runs was 16.7 °C, and the temperature difference in argon-only was 7.5 °C. Therefore, the average temperature difference used in Eq. (1) was 9.2 °C, which resulted in n_O of $3.6 \times 10^{18} \pm 0.1 \times 10^{18}\,\text{m}^{-3}$.

B. O-ring exposure results

Figure 6 shows the rate of mass loss results, in percentage per hour, for all exposure conditions. On any one O-ring sample multiple measurements gave almost identical results, the statistical error smaller than the size of the data point in the figure. Each O-ring material was tested twice, and the results of each of the tests are shown in the figure with the range between them filled in to better represent the uncertainty.

When comparing the O-ring mass loss results between the three cases, it is instructive to compare back to the effect of reactive ion etching (RIE) shown by Coburn and Winters.[19] Like the Coburn and Winters results, the plasma condition, with ions and

12 February 2024 19:37:45

Published under an exclusive license by the AVS

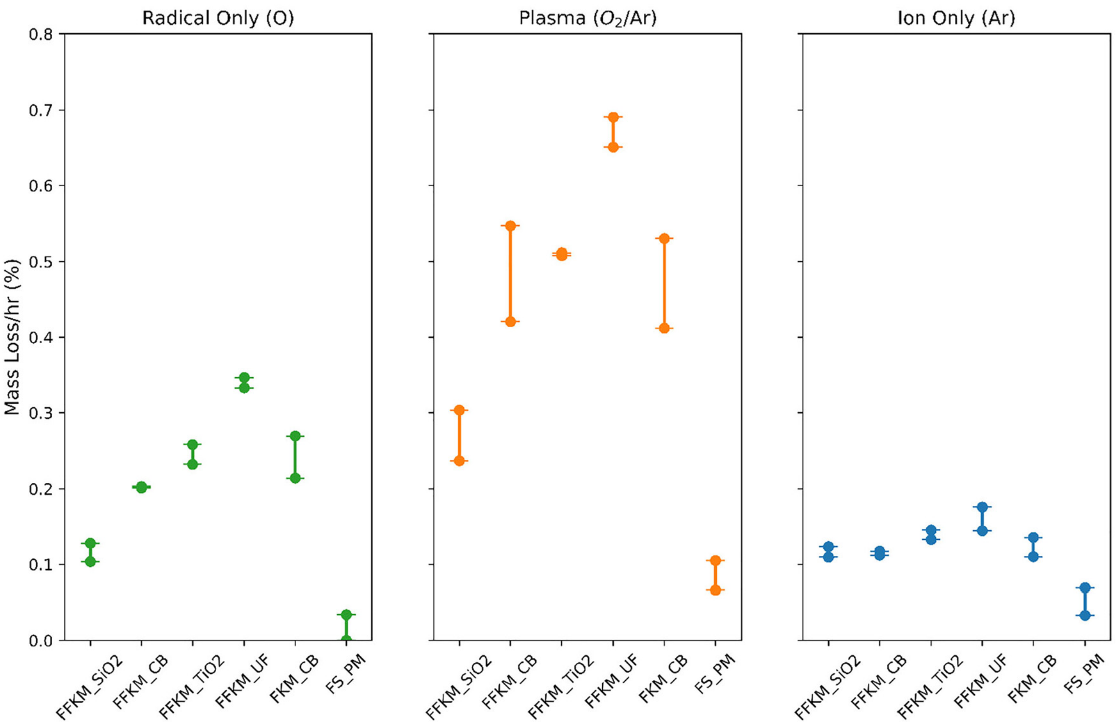

FIG. 6. Mass loss (%) per hour in the radical only, plasma, and ion only exposure conditions. Two samples were tested for each material-condition combination, with the range between the measurements shown.

12 February 2024 19:37:45

radicals, shows the highest mass loss rates across all elastomer materials. In contrast to the Coburn and Winters result, the radical only case still has an appreciable mass loss rate. Interestingly, the radical only condition has similar relative mass loss rates between materials, but the magnitudes of the mass loss rates are 2–3× lower than the plasma case. The ion-only condition does not have the same relative mass loss rates between materials, and overall the mass loss rate does not depend heavily on material, with the exception of FS_PM. The overall differences between conditions indicate that chemical interaction between the plasma and O-rings determines how susceptible the O-rings will be to degradation; it is hypothesized that ions in the plasma then add further energy to the chemical reactions, increasing the degradation rates.

Looking now at the materials, FS_PM had the lowest mass loss rate of all materials to a significant degree. This was not unexpected, as FVMQ fluorosilicones are known to have strong resistance to oxygen plasmas,[10] as the polymer backbone is in practice already an oxide. Among the FFKM/FKM materials, FFKM_SiO_2 had the lowest mass loss rate. Because the backbone of FS_PM is silicon and oxygen and FFKM_SiO_2 has a silica filler, silicon/silica was noted as a common thread for increased resistance to oxygen-containing plasma. Further partition testing would be necessary to test this hypothesis. In all cases, FFKM_UF had the highest mass loss rate. This shows that, although the material is an FFKM, filler materials could aid to increase resistance to degradation from plasma exposure. It was also noted that FKM_CB had a similar mass loss rate to many of the FFKMs. This indicated that in an oxygen plasma environment, FKMs should not be eliminated from consideration at the outset, although the surface analysis shown later in this study does indicate other risks to consider with FKM_CB.

Figure 7 shows the root mean square surface roughness, S_q, of the O-ring materials before exposure and post all exposure conditions. On any one O-ring sample multiple measurements gave almost identical results, the statistical error smaller than the size of the data point in the figure. Each O-ring material was tested twice, and the results of each of the tests are shown in the figure with the range between them filled in to better represent the uncertainty.

The surface roughness of all unexposed materials was similar, with all materials having roughness of 2.5 μm or less on average. After the ion-only exposure, the surface roughness of the materials did not change significantly; FFKM_CB and FFKM_TiO_2 had the largest increases in roughness, with both increasing approximately by a factor of two. There were much more significant surface changes under the radical only and plasma exposures. The surface roughness of FFKM_UF, FFKM_CB, and FFKM_TiO_2 increased significantly in both cases, with FFKM_UF seeing at least a 5× increase. As shown in Fig. 10, a powder formed on FKM_CB instead of surface texturing as with the other materials, so the surface roughness measurement for that material is not a good characterization of surface change as the film appears smooth.

As a general summary, the surface roughness changes were significant in the exposure conditions where oxygen radicals were

Published under an exclusive license by the AVS

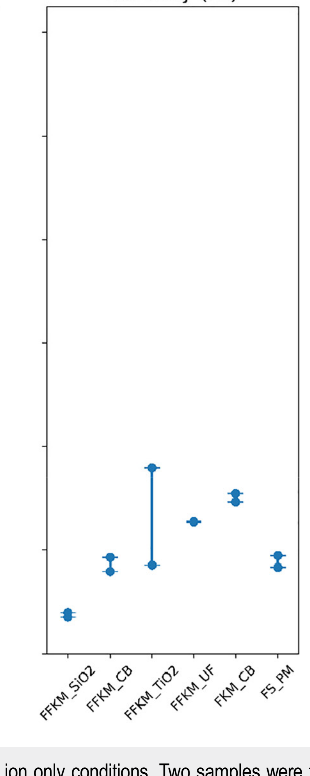

FIG. 7. Root mean square surface roughness (Sq) of unexposed and post exposure O-rings in the radical only, plasma, and ion only conditions. Two samples were tested for each material-condition combination, with the range between the measurements shown.

12 February 2024 19:37:45

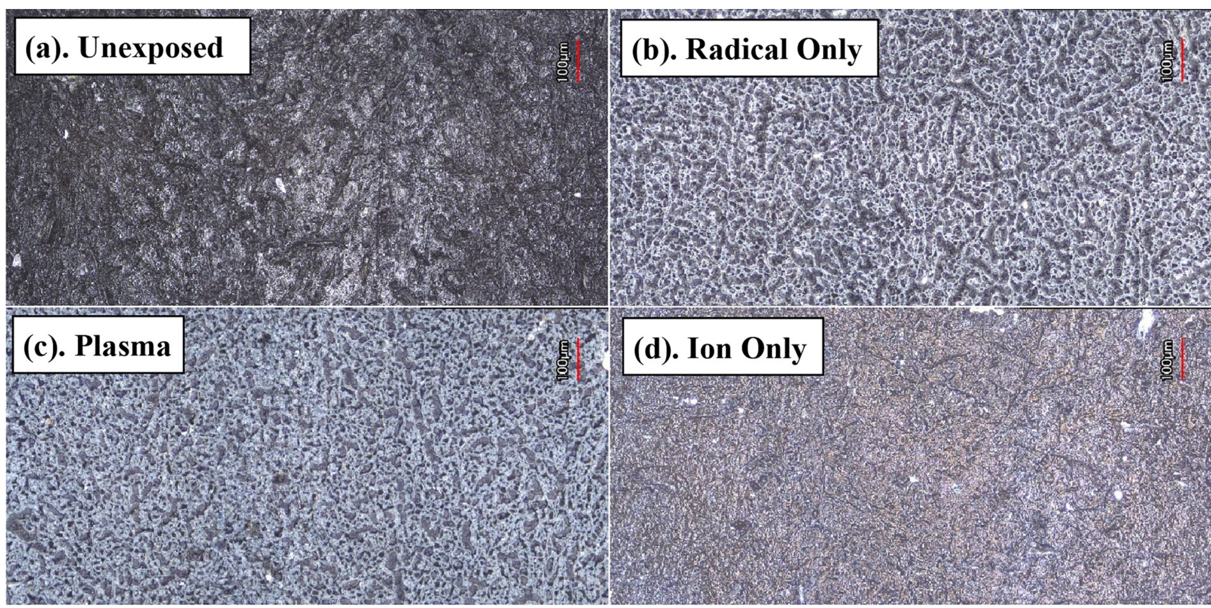

FIG. 8. Optical profilometer images of FFKM_UF at 20× magnification with average Sq value: (a) unexposed, Sq = 1.91 μm; (b) radical only exposure, Sq = 8.23 μm; (c) plasma exposure, Sq = 10.0 μm; and (d) ion-only exposure, Sq = 2.54 μm.

Published under an exclusive license by the AVS

FIG. 9. Optical profilometer images at 20× magnification with average Sq value of: (a) FFKM_SiO_2, unexposed, Sq = 0.482 μm; (b) FFKM_SiO_2, radical only exposure, Sq = 0.597 μm; (c) FFKM_CB, unexposed, Sq = 0.964 μm; (d) FFKM_CB, radical only exposure, Sq = 2.32 μm; (e) FFKM_TiO_2, unexposed, Sq = 1.06 μm; (f) FFKM_TiO_2, radical only exposure, Sq = 4.13 μm; (g) FFKM_UF, unexposed, Sq = 1.91 μm; (h) FFKM_UF, radical only exposure, Sq = 8.23 μm; (i) FKM_CB, unexposed, Sq = 2.47 μm; (j) FKM_CB, radical only exposure, Sq = 2.77 μm; (k) FS_PM, unexposed, Sq = 1.36 μm; and (l) FS_PM, radical only exposure, Sq = 1.48 μm.

12 February 2024 19:37:45

Published under an exclusive license by the AVS

present, indicating that surface changes are primarily radical driven. It is hypothesized that the radicals have higher etch selectivity to some parts of the elastomer over others, whether that is one of the monomers, a part of a monomer, or the crosslinks formed between the polymer chains, which are a different compound than the monomers. The etching product leaves as a volatile compound, and the remaining polymer densifies, contracting in all directions to form the ridges and valleys of the rougher surface. Figure 8 shows optical profilometer images of FFKM_UF unexposed and after all exposure conditions, and the structured surface is seen in both the radical only and plasma conditions. Although the mass loss rate was higher in the plasma condition than radical only condition for all materials, it is noted that the surface roughness is similar in the plasma and radical only conditions. Therefore, there is a limit after which even the densified film is removed. If not, the expectation would be that the surface roughness should have the same trend between conditions as the mass loss rate. In the case of FFKM_UF, the mass loss rate was nearly twice as high in the plasma condition as the radical only condition. However, the surface roughness between those two conditions was similar, indicating that there is a limit to the roughening of the surface.

Figure 9 compares the surfaces of all materials before exposure and after radical only exposure. The comparison of unexposed to radical only was chosen for presentation because most elastomer materials used in the semiconductor industry are in a relatively radical-rich environment, as opposed to a full plasma.

Although it is most clearly seen on FFKM_UF, ridge formation was also present on FFKM_CB and FFKM_TiO_2, to varying degrees. From these differences, it is clear that the specific ingredients of the elastomer—its base polymer, crosslinking system, and filler system—affect the magnitude and length scale of the surface roughening. FFKM_SiO_2 had no discernible surface roughening, indicating that the elastomer erodes uniformly. FS_PM shows some surface degradation, but via a different mechanism, as the surface of the material exhibits cracking on a larger length scale. Similar surface cracking of fluorosilicone elastomers after exposure to atomic oxygen has been reported in the study of degradation of those elastomers in low Earth orbit.[20] FKM_CB showed a negligible change in surface roughness after the exposures containing oxygen radicals. However, a white powder formed on the surface of the elastomer, and so the roughness measurement was actually a measurement of the roughness of this powder. The powder could be easily removed with contact, as shown in Fig. 10, and was measured to be a few micrometers thick. This powder presents a risk of particle contamination in a plasma processing chamber if the powder is removed from the surface of the seal. Further analysis is required to determine the chemical composition and origin of this powder. It is hypothesized to stem from the carbon black filler in FKM_CB, as FFKM_CB showed some white powder formation, albeit to a lesser extent [Fig. 9(d)].

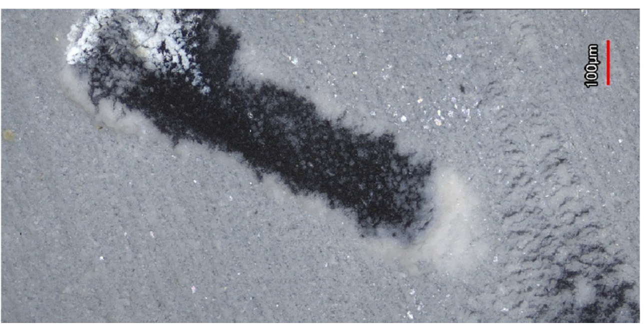

FIG. 10. FKM_CB after exposure to plasma condition, with light physical contact to remove some of powder formed. Powder layer was approximately 5 μm thick.

IV. CONCLUSIONS

Elastomer seals are an essential component used in plasma processing equipment for the semiconductor industry. In plasma environments, these seals degrade over time, with possible failure modes including failure to have a reliable vacuum seal or chamber contamination due to particulate generation. Therefore, the goal of this study was to gain an understanding of the fundamental plasma conditions that drive degradation of elastomer seal materials.

This study used an O_2/Ar plasma chemistry to investigate how plasma interacts and degrades the elastomer materials. The differences in mass loss rates in the plasma, radical only, and ion-only conditions indicate that chemical interaction between the plasma radicals and O-rings determines how susceptible the O-rings will be to degradation; it is hypothesized that ions in the plasma add further energy to the chemical reactions, increasing the degradation rates. The ion-only mass loss rates were relatively low, and did not depend significantly on the material, indicating ions alone are not the driving mechanism of degradation. In the O_2/Ar plasma, the fluorosilicone elastomer had the lowest mass loss rate, the silica-filled FFKM had the lowest mass loss rate among FFKM materials, and the unfilled FFKM had the highest mass loss rate among FFKM materials. The FKM material showed similar mass loss rates to the FFKM materials. It is hypothesized that silicon/silica as a part of the elastomer material, as a backbone material in the fluorosilicone elastomer and the filler in the silica-filled FFKM, caused the increased resistance to oxygen-containing plasma.

It was additionally determined that plasma radicals are the main driver of surface changes of the elastomer, with similar surface roughening in plasma versus radical only conditions and less significant roughening in ion-only conditions. Many FFKMs exhibited surface roughening after exposure to oxygen radicals, with the proposed mechanism being polymer densification as elastomer material components are selectively etched and the etch products volatize. The ion-only case had lower levels of surface roughening, indicating that chemical etching is necessary to drive significant surface change. Finally, although the FKM material had similar mass loss rates to the FFKM materials in O_2/Ar plasma, there was a significant amount of loose particulate generated on the surface of the FKM seal, which could theoretically become a defect source.

ACKNOWLEDGMENTS

This study was conducted at the Center for Plasma-Material Interactions (CPMI) at the University of Illinois at

12 February 2024 19:37:45

Published under an exclusive license by the AVS

Urbana-Champaign. The authors are grateful for funding and support from DuPont. The 3D optical profilometry work was carried out in part in the Materials Research Laboratory Central Research Facilities, University of Illinois.

AUTHOR DECLARATIONS

Conflict of Interest

The authors have no conflicts to disclose.

Author Contributions

Nicholas Connolly: Conceptualization (equal); Data curation (lead); Formal analysis (lead); Investigation (lead); Methodology (equal); Writing – original draft (lead); Writing – review & editing (equal). **Michael Hysick:** Data curation (equal); Investigation (equal). **David E. Barlaz:** Conceptualization (equal); Funding acquisition (supporting); Methodology (equal); Project administration (equal); Supervision (equal); Validation (equal). **Raquel Garza:** Formal analysis (equal); Methodology (equal); Project administration (equal); Supervision (equal). **Gilberto Lunardi:** Formal analysis (equal); Methodology (equal); Resources (supporting); Validation (equal); Writing – review & editing (equal). **David N. Ruzic:** Conceptualization (equal); Formal analysis (supporting); Funding acquisition (lead); Investigation (supporting); Methodology (equal); Project administration (lead); Resources (lead); Supervision (lead); Validation (equal); Writing – review & editing (equal).

DATA AVAILABILITY

The data that support the findings of this study are available from the corresponding author upon request.

APPENDIX: LANGMUIR PROBE ANALYSIS

The RF-compensated, single Langmuir probe described in Sec. II was used to collect current versus voltage (I-V) traces in the plasma condition from Table III. These traces were analyzed to determine the electron temperature (T_e) and density (n_e) of the plasma, following the method described in Ruzic's *Electric Probes for Low Temperature Plasmas*.[18] Figure 11 shows a representative I-V trace, with the floating potential and plasma potential noted on the plot. The floating potential is found where the ion current equals the electron current. The plasma potential is located at the inflection point (the "knee") of the electron current-dominated region of the trace, which is noted in Fig. 11 by a minimum in the first derivative of a polynomial fit to the I-V trace. With the floating and plasma potentials determined, the electron temperature (T_e) was determined by analyzing the slope of the linear approximation of the natural log of the electron current versus the difference of plasma potential and probe voltage, as shown in Fig. 12 for the representative I-V trace in Fig. 11. The electron temperature (in eV) is the negative reciprocal of the slope. It is noted that the experimental data in Fig. 12 is not exactly linear, which indicates the electron energy distribution is not Maxwellian. The Laframboise method was used to determine plasma density (n_e), as sheath size and sheath collisionality affect the analysis of the collected current.[18] T_e was determined to be 4.6 ± 0.1 eV and n_e was determined to be $2.9{\cdot}10^{16} \pm 0.07 \times 10^{16}\,\mathrm{m^{-3}}$, with standard deviations determined from 15 measurements.

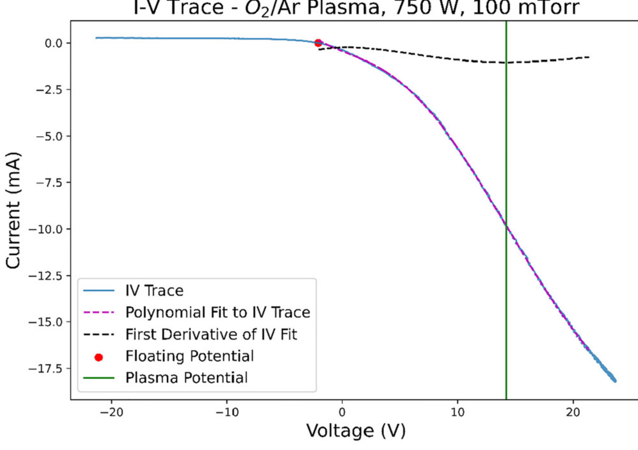

FIG. 11. Representative current vs voltage trace collected with an RF-compensated, single Langmuir probe in the plasma condition from Table II.

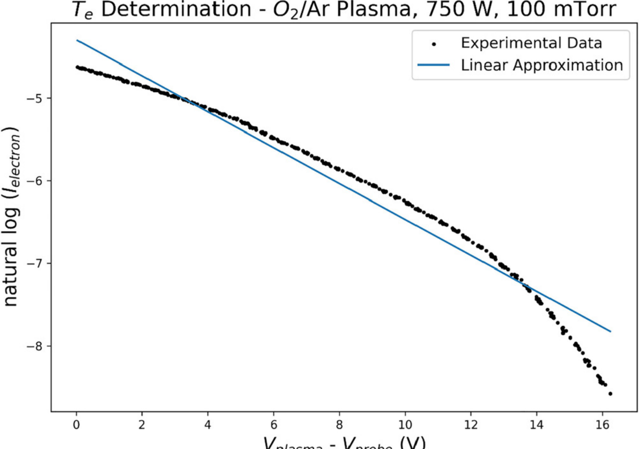

FIG. 12. Natural log of the electron current vs the difference of the plasma potential and the probe voltage for the I-V trace in Fig. 11.

REFERENCES

[1] M. Gulcur and K. Beekmann, *2016 International Symposium Semiconductor Manufacturing (ISSM)* (IEEE, Tokyo, 2016), pp. 1–4.
[2] M. A. Lieberman and A. J. Lichtenberg, *Principles of Plasma Discharges and Materials Processing*, 1st ed. (Wiley, New York, 2005).
[3] T. S. Reger and G. J. Reichl, in *2020 31st Annual SEMI Advanced Semiconductor Manufacturing Conference (ASMC)*, Saratoga Springs, NY, 24–26 August 2020 (IEEE, New York, 2020), pp. 1–5.
[4] T. Goto, S. Obara, T. Shimizu, T. Inagaki, Y. Shirai, and S. Sugawa, J. Vac. Sci. Technol. A **38**, 013002 (2020).
[5] A. Verschuere and E. Cole, Rubber Fibres Plastics Intl. **10**, 122 (2015).
[6] B. Améduri, B. Boutevin, and G. Kostov, Prog. Polym. Sci. **26**, 105 (2001).

12 February 2024 19:37:45

Published under an exclusive license by the AVS

[7]J. Scheirs, *Modern Fluoropolymers: High Performance Polymers for Diverse Applications* (Wiley, Chichester, 1997).
[8]S. Wang and J. M. Legare, J. Fluor. Chem. **122**, 113 (2003).
[9]W.-Y. Zhuo, Q.-L. Wang, G. Li, G. Yang, H. Zhang, W. Xu, Y.-H. Niu, and G.-X. Li, Chin. J. Polym. Sci. **40**, 504 (2022).
[10]See https://www.momentive.com/docs/default-source/productbycategorydocument/elastomers/momentive-elastomers-fluorosilicones-brochure.pdf for "Fluorosilicones," Momentive.
[11]J. M. Legare, S. Wang, M. Vigliotti, and S. Sogo, in *2008 IEEE/SEMI Advanced Semiconductor Manufacturing Conference*, Cambridge, MA, 5–7 May 2008 (IEEE, New York, 2008), pp. 297–300.
[12]W. B. Alexander and J. Foggiato, in *2008 IEEE/SEMI Advanced Semiconductor Manufacturing Conference*, Cambridge, MA, 5–7 May 2008 (IEEE, New York, 2008), pp. 123–126.
[13]G. R. Tynan *et al.*, J. Vac. Sci. Technol. A **15**, 2885 (1997).
[14]D. Qerimi, I. Shchelkanov, G. Panici, A. Jain, J. Wagner, and D. N. Ruzic, J. Vac. Sci. Technol. A **39**, 023003 (2021).
[15]D. Qerimi, G. Panici, A. Jain, D. Jacobson, and D. N. Ruzic, J. Vac. Sci. Technol. A **39**, 023004 (2021).
[16]D. Qerimi, "Radical probe system for in-situ measurements of radical densities of hydrogen, oxygen and nitrogen," M.S. thesis (University of Illinois at Urbana-Champaign, 2019).
[17]A. Vesel and M. Mozetic, J. Phys. Conf. Ser. **162**, 012015 (2009).
[18]D. N. Ruzic, *Electric Probes for Low Temperature Plasmas* (American Vacuum Society, New York, 1994).
[19]J. W. Coburn and H. F. Winters, J. Appl. Phys. **50**, 3189 (1979).
[20]A. Laikhtman, I. Gouzman, R. Verker, E. Grossman, and H. G. Pippin, High Perform. Polym. **20**, 447 (2008).

12 February 2024 19:37:45

Published under an exclusive license by the AVS